Ferromagnetic resonance excitation of two-dimensional wall structures in magnetic stripe domains

U. Ebels, L. Buda, and K. Ounadjela
Institut de Physique et Chimie des Matériaux de Strasbourg, 23 rue du Loess, F-67037 Strasbourg Cedex, France

P. E. Wigen
Department of Physics, Ohio State University, 174 West 18th Avenue, Columbus, Ohio 43210
(Received 7 July 2000; revised manuscript received 15 November 2000; published 13 April 2001)

Using ferromagnetic resonance, an experimental approach is presented to evidence and analyze the small amplitude excitations of inhomogeneous magnetization distributions in thin magnetic films. This approach is applied to the complex two-dimensional (2D) domain walls of Co(0001) stripe domains, which contain a reduced Bloch part in the film center and extended flux closure caps at the film surface. Upon varying the pumping field orientation, the different regions of the domain walls, the flux closure caps and the domains can be selectively excited, yielding a rich excitation spectrum with up to seven modes. In combination with static investigations and 2D micromagnetic simulations these modes can be assigned to the domain-wall resonance modes, the oscillations of the flux closure caps, as well as to the excitation of the domain magnetization.

DOI: 10.1103/PhysRevB.63.174437 PACS number(s): 76.50.+g, 75.60.Ch, 75.40.Mg, 75.70.Ak

I. INTRODUCTION

The application of small magnetic film elements in high-density data storage technologies demands a fundamental understanding of their static and dynamic magnetic properties. The dependence of the static spin distribution on the thin-film geometry (shape, thickness, and lateral extension) is only one example.[1] Small perturbations to the static configuration are described by spin waves and can be excited either thermally[2,3] or externally by an oscillating high-frequency field.[4,5] Such excitations have been studied in the past for magnetic thin-film or multilayer systems dominantly in the magnetic homogeneous or saturated state where the magnetization distribution is uniform inside the magnetic material.[2–5]

Here, an experimental approach using ferromagnetic resonance is presented to analyze the excitation spectra of nonhomogeneous magnetization distributions whose magnetic units are in the submicrometer range. A model system for this is the stripe domain structure supported in perpendicular Co(0001) thin films.[6] In this case the domain regions are separated by broad two-dimensional (2D) domain walls which extend far into the domain region.[7–9] Their profile varies across the film thickness being Bloch-like in the film center and containing pronounced Néel-type ''flux closure caps'' at the film surface.[7] A schematic of this stripe domain structure is shown in Fig. 1.

Generally, stripe domains develop in thin films having a uniaxial anisotropy K_u whose easy axis is oriented perpendicular to the film plane.[10,11] An important property that characterizes the magnetization distribution inside stripe domains is the Q factor[7] where Q is defined as the ratio between the uniaxial anisotropy energy K_u and the demagnetization field energy $2\pi M_s^2$, $Q=K_u/(2\pi M_s^2)$. For the Co(0001) thin films studied here, the Q factor is smaller than 1, $Q\cong 0.5$.[6] From the presented micromagnetics calculation it is derived that in this case the flux closure caps assume a rather large volume fraction of up to 35%. Besides the excitation of the magnetization inside the domain regions it is therefore expected that the flux closure regions also give rise to measurable absorption peaks in the ferromagnetic resonance (FMR) excitation spectra.

As indicated in Fig. 1, the different parts of the complex 2D wall structure can be selectively excited upon varying the

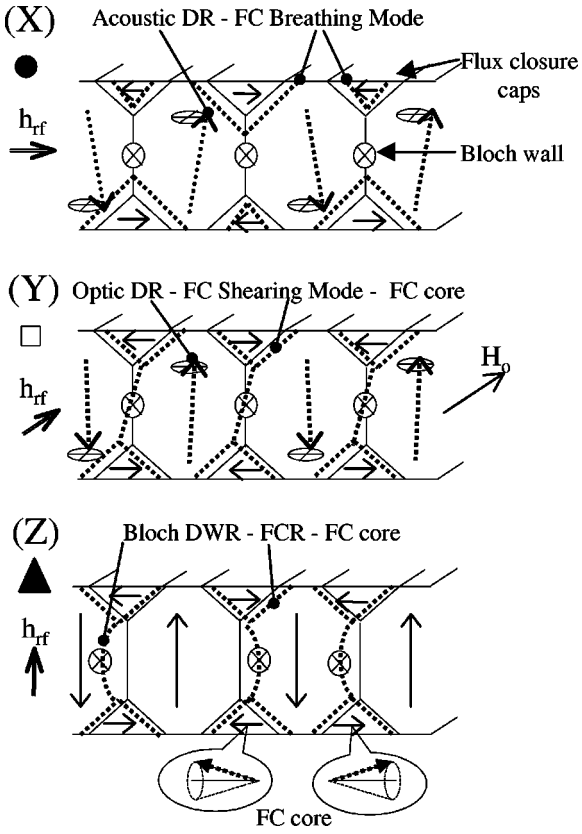

FIG. 1. Schematic of the static, zero-field flux closure stripe domain structure of Co(0001) (solid lines) and the pumping scheme for the three different pumping field configurations *X*, *Y*, and *Z*. The dotted lines and arrows denote a snapshot of the oscillations of the magnetization corresponding to the different modes excited at low bias field in the given pumping field configuration.

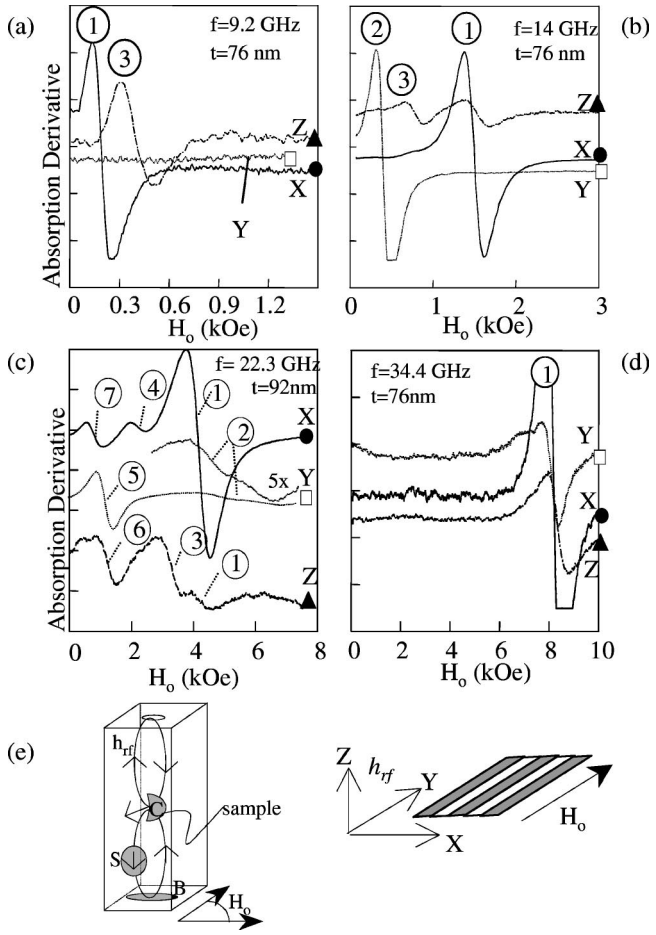

FIG. 2. The absorption derivative spectra for four different frequency bands: (a) *X* band (9.2 GHz), (b) Ku band (14 GHz), (c) *K* band (22.3 GHz), and (d) *Q* band (34.4 GHz). The thickness *t* of the Co(0001) films is indicated inside each figure. The labels (1) to (7) denote the various modes, each number corresponding to the same type of mode at the respective frequencies. Configurations *X* and *Y* represent the same intensity scale, whereas the spectra in configuration *Z* were taken at a higher sensitivity level of the FMR spectrometer (typically 2*x* to 10*x* higher). (e) The magnetic field distribution (full line) in a TE_{102} rectangular cavity and the different sample positions, denoted by B=bottom, S=side wall, and C=center of the cavity. The applied bias field orientation can be rotated through 360°. The sketch to the right indicates the three different pumping field configurations *X*, *Y*, and *Z* as defined in Fig. 1 as well as the orientation of the bias field H_o with respect to the stripe domain orientation.

orientation of the pumping field h_{rf} from: (*X*) in-plane-perpendicular to the stripes to (*Y*) in-plane-parallel to the stripes and further to (*Z*) perpendicular to the film plane. Applying this concept to the low-*Q* Co stripe domain structure, a rich excitation spectrum with a total of seven modes is evidenced, as shown in Fig. 2. The systematic study of the frequency and thickness dependence of this excitation spectrum in combination with static 2D micromagnetic calculations permit us to attribute two of these modes to the conventional acoustic and optic domain resonance (DR) modes and a third mode to the domain-wall resonance mode (DWR), while the remaining modes are attributed to the excitation of the flux closure caps.

The paper is structured as follows. In Sec. II, the sample preparation is described. In Sec. III the static magnetic properties are discussed. In Sec. IV the FMR results are described followed by a brief discussion in Sec. V. In Sec. VI the domain resonance modes are analyzed and in Sec. VII the modes associated with the domain wall and flux closure caps.

II. SAMPLE PREPARATION

A series of thin-film structures with a layering of mica/Ru (56 Å)/Co(t)/Ru (32 Å) was prepared by *e*-beam evaporation in ultrahigh vacuum, with a Co layer thickness *t* ranging from 12 to 100 nm in 8-nm steps. The Co layers were deposited on mica substrates with a Ru buffer layer that was grown at 700 °C, while the Co was grown at a temperature of 400 °C. A Ru cap layer was deposited (at room temperature) to prevent oxidation. *In situ* reflection high-energy electron diffraction (RHEED) as well as *ex situ* x-ray diffraction confirm the hcp structure and high crystalline quality throughout the film thickness.[12] Furthermore, the x-ray-diffraction measurements show that diffusion at the interfaces is less than 6 Å, which should not distort or change the magnetic properties of the cobalt layer.[6]

III. STATIC PROPERTIES

A. In-plane remanence, saturation fields, and *Q* factor

The thickness range investigated here, between 20 and 100 nm, covers the reorientation of the magnetization from in-plane at small $t<28$ nm to out of plane at large $t \geqslant 60$ nm. This magnetization reorientation has been established by superconducting quantum interference device (SQUID) magnetometry (Quantum Design) and by magnetic force microscopy (MFM) imaging (Digital Instruments Dimension 3000). From the MFM measurements the domain width *L* was estimated, which lies in the submicron range with $L=45$–100 nm for $t=28$–100 nm. From the SQUID measurements the saturation magnetization M_s and the saturation field in plane ($H_{sat\|}$) and out of plane ($H_{sat\perp}$) were deduced. For all samples, M_s is independent of the film thickness and close to the bulk value with an average value of $(1.39\pm 0.1)10^3$ emu/cm^3. Details of the MFM images and the thickness dependence of *L* as well as typical hysteresis loops can be found in Ref. 6. Here, only the thickness dependence of the in-plane remanence ratio and the saturation field values $H_{sat\|}$ and $H_{sat\perp}$ are considered.

The stripe domain structure is induced by first saturating the film in an in-plane field and then reducing the field to zero.[6] From the corresponding in-plane remanence ratio M_R/M_S at zero field, three regions can be distinguished which describe the magnetization reorientation from out of plane to in plane upon reducing *t*; see Fig. 3(a):

•Region I for $t \geqslant 60$ nm corresponding to perpendicularly magnetized ''up'' and ''down'' stripe domains with low remanence of 20–25 %, arising from the canted spins inside the domain wall.

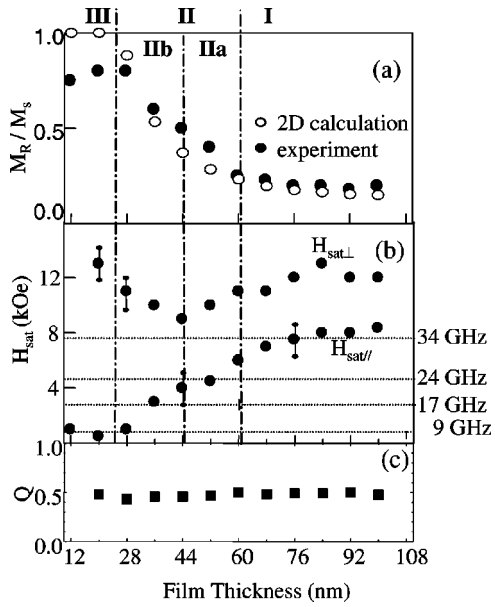

FIG. 3. (a) The in-plane remanent magnetization ratio M_R/M_s as a function of *t*. The full dots denote experimental results while the open circles are results from 2D micromagnetic simulations. (b) The in-plane $H_{sat\parallel}$ and out-of-plane $H_{sat\perp}$ saturation field values. The dotted horizontal lines correspond to the in-plane uniform mode resonance fields at the given frequency values. The subdivision of the thickness range into regions I, IIa, IIb, and III is described in the text. (c) The experimentally determined *Q* factor.

•Region II for $20<t\leqslant 60$ nm with linearly increasing remanence (25–80 %) indicating a canted magnetization state of the domain magnetization.

•Region III for $t\leqslant 20$ nm with high remanence (80%) and in-plane magnetization.

Besides establishing the thickness range over which the stripe domain structure is stabilized it is furthermore important to establish the corresponding field range. The saturation field values $H_{sat\parallel}$ and $H_{sat\perp}$ for in-plane and out-of-plane magnetization procedures are shown in Fig. 3(b). To note is that $H_{sat\parallel}$ decreases continuously with decreasing *t*, whereas $H_{sat\perp}$ first decreases, but then increases below $t=44$ nm. The kink at 44 nm indicates a change in the perpendicular remagnetization procedure. Above 44 nm the saturation is achieved through a domain-wall motion process by which one type of domain grows while the other one shrinks.[11] Below 44 nm the increased canting of the magnetization into the film plane changes the perpendicular remagnetization process to a dominantly rotational reorientation. The canted thickness range II of Fig. 3 can thus be subdivided into two regions in which the out-of-plane (region IIa) and the in-plane (region IIb) magnetization components respectively dominate the magnetic properties.

For the interpretation of the FMR spectra, the relative position of the resonance field H_{res} to the saturation field is important. It is found that for a bias field applied perpendicular to the film plane the resonance field is larger than the saturation field value and can be described by the perpendicular uniform mode resonance ($H_{res}\geqslant 12$ kOe at *X* band and $H_{res}\simeq 16$ kOe at *K* band). From this, the anisotropy field strength $H_u=2K_u/M_s$ is estimated using the perpendicular uniform mode resonance condition[13] and the value of M_s deduced from SQUID measurements. H_u is found to be constant for the thickness range investigated with an average value of $H_u=(8.5\pm 0.5)$ kOe. This leads to a thickness independent *Q* value of $Q\cong 0.5$ as shown in Fig. 3(c).

In contrast to the perpendicular resonance, the parallel resonance fields (applied in plane and parallel to the stripes) are lower than the saturation field values. As a comparison, in Fig. 3(b) the horizontal dotted lines denote the resonance field values of the in-plane uniform mode, revealing that H_{res} is smaller than H_{sat} below *Q* band (34 GHz) and above a certain thickness. This corresponds to the frequency and thickness range for which the stripe domain excitations have been investigated here.

B. Relative volume fraction of the domains, flux closure caps, and the Bloch wall height

The static experiments provide information only on the average magnetization, but not on the internal magnetization distribution. Therefore 2D periodic micromagnetics calculations were employed in order to estimate the relative volume fraction of the domain magnetization of the flux closure caps as well as the height of the Bloch domain wall. Details of these calculations are summarized in the Appendix. The material parameters used correspond to those determined from the static experiments for the Co(0001) films with $Q=0.5$.

In Fig. 4(a) the magnetization distribution across the film thickness and one domain period is shown for a $t=100$-nm film at zero field. The domain regions and flux closure regions are clearly visible and are more pronounced when plotting the contour map of the normalized component $m_x=M_x/M_s$ in Fig. 4(b), since only inside the flux closure caps the magnetization is rotated towards the *x* direction.

From the magnetization distribution of Fig. 4(a), the in-plane remanence at zero field is determined as the average normalized component $\langle m_y\rangle=\langle M_y/M_s\rangle$. Its thickness dependence is in agreement with the experimental data as shown in Fig. 3(a) (open circles). The reorientation of the magnetization in the three regions I, II, and III from in plane towards out of plane derived from the in-plane remanence of Fig. 3(a) is confirmed by the evolution of the domain magnetization angle θ_D (here with respect to the film plane). From the graphic to the right of Figs. 4(a) and 4(b) it is seen that the domain angle θ_D (crosses), averaged over the domain center line, varies only very weakly with *t* in region I ($\theta_D\simeq 90°$). In region IIa a slight canting sets in ($\theta_D=80$–$90°$), which becomes very strong in region IIb below 44 nm.

For the interpretation of the FMR experiments, an estimate of the relative volume fraction of the domains V_d, of the flux closure caps V_{FC} as well as of the relative height of the Bloch wall t_B/t are required as well as their respective evolution with thickness and applied bias field (in-plane and parallel to the stripes). Here we concentrate on the thickness range $t>44$ nm, the region in which the perpendicular domain magnetization and hence the stripe domain properties dominate. In this thickness range V_d and V_{FC} can be esti-

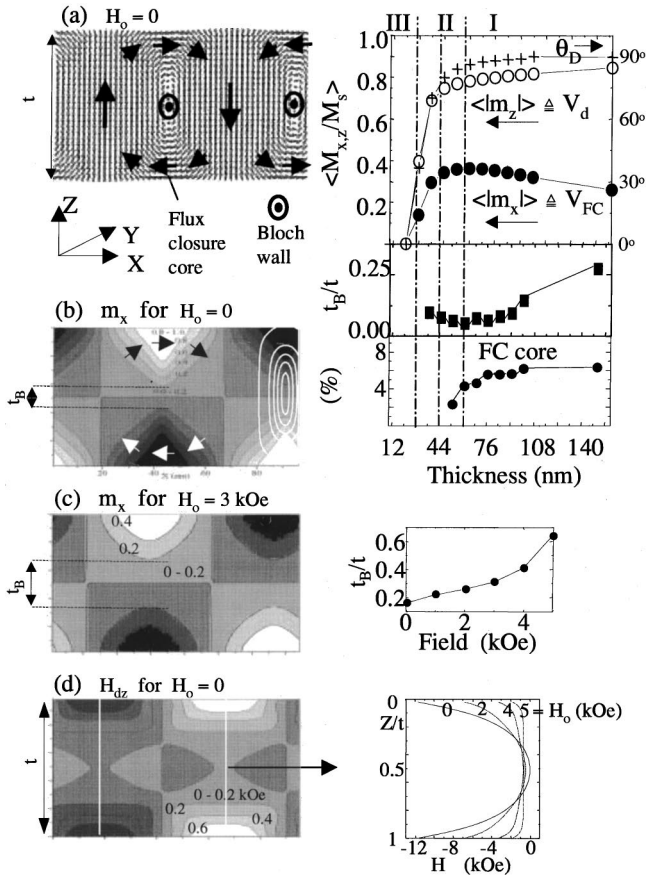

FIG. 4. (a) Spin configuration of a 100-nm-thick Co film according to 2D micromagnetic calculations, indicating the flux closure caps and Bloch domain-wall parts. To the right are shown the thickness dependence of the domain angle θ_D (crosses), the domain volume V_d (open circles), the flux closure cap volume V_{FC} (full dots), the zero field relative Bloch wall height t_B/t (open squares), and the flux closure core volume (full dots). (b) and (c): contour map of the magnetization component m_x for $t=100$ nm at (b) $H=0$ kOe and (c) $H=3$ kOe. The white contour lines in (b) correspond to the magnetization component m_y which describe the Bloch wall. The center contour denotes $m_y=0.9$ and each contour line decreases by 0.2. The field dependence of the relative Bloch wall height t_B/t is shown to the right. (d) Contour map of the z component of the demagnetization field H_{dz} and the variation of H_{dz} along the domain center line for different bias field values H_o.

mated from the average of the normalized magnetization components as $V_d=\langle|m_z|\rangle$ and $V_{FC}=\langle|m_x|\rangle$, respectively. Upon decreasing t, the flux closure caps extend further into the film across the thickness as well as into the domain regions. Consequently their relative volume fraction V_{FC} increases from 25 to 35 % for $t=150$–44 nm as shown in the diagram to the right of Figs. 4(a) and 4(b). At the same time V_d decreases from 85 to 75 %, remaining, nevertheless, the largest contribution in this thickness range. Furthermore, the increase of V_{FC} reduces the relative Bloch height t_B/t, from 30% at $t=150$ nm to almost zero at 60 nm as shown in the diagram to the right of Figs. 4(a) and 4(b). Here t_B/t was estimated from the contour line of $m_x=0.2$ ($m_y=0.98$) of the contour maps such as shown in Fig. 4(b). At $t=60$ nm the zero field Bloch height collapses and the wall consists only of flux closure caps.

The extended flux closure caps contain an almost domain-like region in the center with horizontal magnetization ($\|x$) at the film surface. The relative volume fraction of this flux closure core is about 5–6 % ($t>60$ nm) as estimated from the contour line $m_x>0.9$ shown in Fig. 4(b).

The variation of the magnetization profile as a function of an applied field (in plane and parallel to the stripes) is illustrated for the m_x contour map in Fig. 4(c) for $H=3$ kOe. In comparison to Fig. 4(b) it is seen that upon increasing the field, the region of strong m_x component is reduced. In particular inside the flux closure caps the magnetization rotates from the Néel direction into the Bloch direction, smoothing the profile across the thickness and enhancing effectively the Bloch height as indicated in the diagram to the right of Fig. 4(c). Similarly, when regarding the variation of the perpendicular component of the internal demagnetization field H_{dz} across the domain center line [deduced from the contour map shown in Fig. 4(d)], it is seen that at zero field H_{dz} varies parabolic across the film thickness but flattens in an applied field.

IV. EXPERIMENTAL EXCITATION SPECTRUM

A. Pumping scheme

In FMR a precession of the magnetization around its equilibrium position is induced by a weak microwave pumping field h_{rf}. This excitation is only effective when the local torque is nonzero, $\mathbf{M}\times\mathbf{h}_{rf}\neq 0$. Using this condition, it follows that the different regions of the configuration shown in Fig. 4 can be selectively excited upon varying the pumping field orientation. This leads to the three possible pumping configurations shown in Fig. 1.

•In pumping configuration (X), h_{rf} lies in the film plane and perpendicular to the stripes and couples to the spins inside the domains, the Bloch domain wall, and the canted spins inside the flux closure caps (but not to the flux closure core).

•In pumping configuration (Y), h_{rf} lies in the film plane and parallel to the stripes, and couples to the spins inside the domains and to all spins inside the flux closure caps, but not to the Bloch domain-wall spins.

•In pumping configuration (Z), h_{rf} lies out of the film plane and couples to the spins inside the Bloch domain wall and the flux closure caps but not to the domain spins.

These pumping configurations are realized in a TE_{102} rectangular cavity as shown in Fig. 2(e). It is noted that the induced stripe structure shows a rotatable in-plane anisotropy, which means that the stripe domains are always induced parallel to the in-plane saturation field irrespective of its orientation to a given in-plane crystal axis. In this way, h_{rf} can be varied continuously from the (X) to the (Y) configuration when placing the sample at position B given in Fig. 2(e).

B. Frequency and thickness dependence

Frequency dependence. Typical FMR derivative spectra for all three pumping configurations (X), (Y), and (Z) and

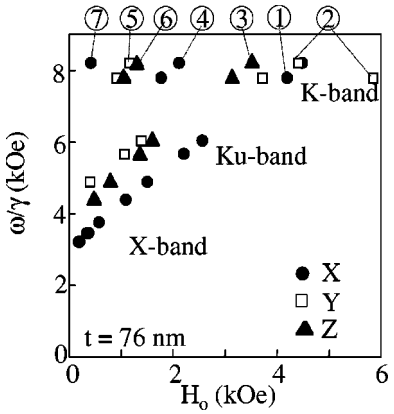

FIG. 5. (a) The experimentally determined frequency-field dispersion for a $t=76$-nm Co film in the three pumping field configurations *X*, *Y*, and *Z* defined in Fig. 1. The notation $X=$ full dot, $Y=$ open square, and $Z=$ full triangle is used throughout the paper in all figures.

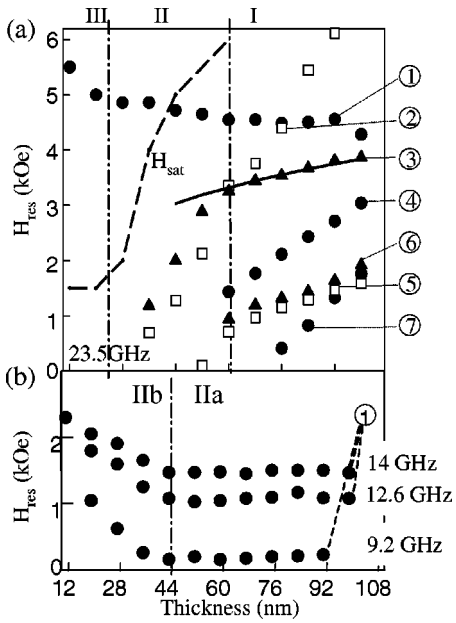

FIG. 6. (a) The experimentally determined thickness dependence of the resonance fields at $f=23.5$ GHz for modes (1) to (7). The dashed line denotes the saturation field vs thickness. The full line across mode (3) is the Bloch domain-wall resonance mode calculated from a 1D model (Ref. 18) for ideal stripe domains as described in the text. (b) The thickness dependence of the resonance fields for mode (1) at $f=9.2$, 12.6, and 14 GHz.

for an in-plane bias field parallel to the stripes are shown in Figs. 2(a)–2(d) for four different frequency bands. For each FMR field sweep at constant frequency, the domain structure was induced anew by first saturating the film in plane, then reducing the field to zero and subsequently sweeping into the direction of the saturation field. The number of modes varies considerably with the frequency. At *X* band, two modes are seen, one each in configuration (*X*) and (*Z*). At Ku band three modes are observed, one for each pumping configuration. At K-band up to seven modes can be seen and at *Q* band only one mode is seen.

The labeling of the modes is derived from the spectrum at *K* band going from high to low fields. In detail, the modes observed at *K* band in configuration (*X*) are labeled (1), (4), and (7), those in configuration (*Y*) are labeled (2) and (5), and those in configuration (Z) are labeled (3) and (6). It is noted, that mode (1) at all frequencies is the highest intensity mode and therefore indicates that it is essentially the same mode. For all other modes the intensity is approximately 1/10 of mode (1) except for mode (2) at Ku band which is of equal intensity; see Fig. 2.

The complete frequency-field ($\omega-H$) dispersion was obtained from measurements at ten frequencies: 9.2, 9.9, 10.75, 12.5 GHz (*X* band); 14, 16, 17.5 GHz (Ku band); 22.3, 23.5 GHz (*K* band); and 34 GHz (*Q* band). For each frequency band the length of the rectangular cavity was adjusted to tune to the desired frequency. Figure 5 reveals a positive and almost linear dispersion for most of the modes which justifies their labeling in the different spectra given in Fig. 2. In particular it shows a smooth and continuous dispersion of the highest intensity mode (1), which is the only mode seen to continue to *Q* band (and therefore not shown in Fig. 5). Similarly, mode (3) shows an almost linear dispersion. In contrast, mode (2) is only linear at lower frequencies, then starts to cross mode (3) and mode (1) and indicates a change from a positive to a negative slope at *K* band. The low-field modes (4) to (7) set in at the upper Ku-band edge and also indicate a positive dispersion. It is furthermore noted that this $\omega-H$ dispersion is the same in character for all thicknesses, differing only in the precise values of the resonance fields.

Thickness dependence. At higher frequencies (*K* band), the resonance fields of modes (1) and (2) shown in Figs. 2 and 5 are very close and the question may arise whether it is the same mode which is weakly excited at both pumping field configurations (*X*) and (*Y*). However, from the thickness dependence of H_{res} shown in Fig. 6(a) for $f=23.6$ GHz these modes develop very differently. While the resonance field H_{res} of mode (1) is almost constant, H_{res} of mode (2) as well as of all other modes decreases linearly (with different slopes) upon decreasing thickness. Of particular note is the drastic change in the slope of modes (3) to (7) below $t=60$ nm, which coincides with the boundary between region I and II, see Figs. 3 and 4, at which the canting of the domain magnetization into the film plane sets in.

V. DISCUSSION

In the past, the dynamic properties of stripe domains have been studied intensively, experimentally, and theoretically, for high-*Q* magnetic oxides such as Garnet and Ferrite films (bubble materials),[14–20] however, not many investigations are reported in the case of low-*Q* materials.[9,21,22] In the limit of high-*Q* values (negligibly thin, 1D Bloch walls) two fundamental excitations exist: the domain resonance mode (DR) which contains an acoustic and an optic branch,[17–19] and the Bloch domain-wall resonance mode (BDWR).[16,18,20] These modes will also be present in the stripe domain structure of

the Co films, however, the presence of the flux closure caps will modify the resonance frequencies (and resonance fields) as well as the domain-wall resonance mode character.

Before addressing the possible character of the observed modes, it should be mentioned that the resonance field of all modes shown in the $\omega - H$ dispersion in Fig. 5 is smaller than the in-plane saturation field ($H_{sat\|} = 7.5$ kOe for $t = 76$ nm). Similarly, in Fig. 6(a) the resonance field of all modes is lower than the saturation field $H_{sat\|}$ (dashed line), except for mode (1) below 44 nm. Therefore these modes have to be associated with the stripe domain structure and will be analyzed in the following in this respect. In addition, the visibility of these modes only in a specific pumping field configuration indicates that they are features intrinsic to the complex magnetization distribution of the stripe domain structure. The very systematic thickness and frequency dependence of these modes therefore reflects the changes of the local internal fields with thickness and applied bias field.

It is also mentioned that additional measurements with the bias field varying from in plane to out of plane reveal that only modes (1) and (2) continue to the uniform mode resonance of the perpendicular saturated state, while all other modes decrease in intensity and vanish at some intermediate field angle. Moreover, at perpendicular resonance with $H_{res} > H_{sat\perp}$ no indication for the excitation of exchange modes across the film thickness is observed.

Finally, the multiplicity of the modes is not consistent with interface inhomogeneities or with a restricted penetration depth of the h_{rf} field due to a finite skin depth. The skin depth at resonance lies on the order of several tens of a nanometer,[23] which guarantees excitation of the flux closure cap spins as well as the domain center spins.[24] However, effects of surface pinning and the finite skin depth should be considered for an exact evaluation of the resonance conditions and extraction of magnetic parameters.[23] This lies beyond the scope of this work. More important is to arrive first at a qualitative understanding of the fundamental character of the various modes.

VI. DOMAIN RESONANCE MODES

A. Acoustic and optic domain modes

Considering first the domain resonance (DR) modes. In the case of high-Q materials ($Q > 1$) with nearly pure Bloch domain walls, the up and down domains are regions whose magnetization and internal fields can be considered as almost uniform. Hence the magnetization inside the domains can perform a uniform modelike precession, where the precessions in adjacent domains are coupled via dipolar fields, leading to an acoustic and optic domain resonance branch.[17–19] These domain resonance modes can be selectively excited by the pumping configurations (X) or (Y) as indicated in the pumping scheme of Fig. 1. This selective excitation is based on the requirement that energy is absorbed only when the total dynamic moment $\mathbf{m}_{tot}$ has a component parallel to the pumping field, $\mathbf{m}_{tot} \cdot \overline{\mathbf{h}}_{rf} \neq 0$.[25] For a definition of $\underline{\mathbf{m}}_{tot}$, see the top view in Fig. 7 showing snapshots of the precessional motion.

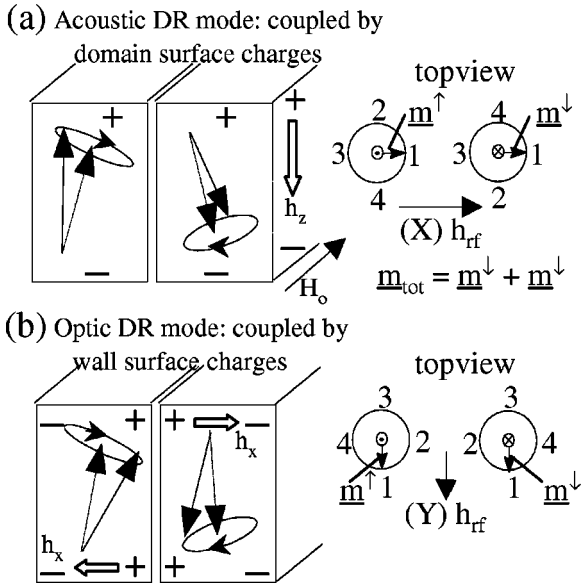

FIG. 7. A schematic illustration of the precession of the domain magnetization for (a) the acoustic and (b) the optic domain resonance mode. The plus and minus signs indicate the dynamic charges giving rise to the dynamic dipolar fields h_z and h_x. The top view to the right indicates the precessional motion of the dynamic moments $\underline{\mathbf{m}}^{\uparrow,\downarrow}$ as seen from the top surface. $\underline{\mathbf{m}}^{\uparrow}$ of the left domain precesses counterclockwise and $\underline{\mathbf{m}}^{\downarrow}$ of the right domain precesses clockwise.

In the acoustic DR mode the magnetization in both domains is in phase perpendicular to the walls [positions 1 and 3 of topview Fig. 7(a)], while it is out of phase in positions 2 and 4. The latter positions lead to a variation of the domain surface charges, indicated by the plus and minus signs, which give rise to the dynamic dipolar coupling field h_z, indicated by the open arrow. These dynamic dipolar fields add to the restoring torque and enhance the precession frequency. In a similar way, the out of phase precession at positions 2 and 4 for the optic mode, Fig. 7(b), leads to a charging of the domain walls ($\nabla \vec{M} \neq 0$ across the wall) and a dipolar coupling field h_x which is in phase with the restoring torque and thus enhances the resonance frequency.

It is noted that the assignment of the acoustic and optic DR mode is chosen with respect to the applied bias field H_o orientation, in plane and parallel to the stripes. It guarantees that the acoustic mode continues as the uniform FMR mode, when for a large enough in-plane bias field the stripe domain structure is wiped out and the film is uniformly in-plane magnetized.

B. Domain resonance modes in Co(0001)

From the seven modes observed for Co(0001) at K-band frequencies (23 GHz) (see Figs. 2, 5, and 6), modes (1) and (2) are identified as the acoustic and optic domain resonance modes, respectively. This assignment is based to one part on the pumping field configuration in which these modes are excited (compare Fig. 1) and to another part on the following:

• As shown in Fig. 4(a), the domains take up the largest volume fraction of the spin configuration ($>75\%$ for $t>44$ nm). Consequently, the DR modes should give rise to the strongest absorption peaks. From Fig. 2 it can be seen that mode (1) in configuration (*X*) is the highest intensity mode at all frequencies whereas mode (2) in configuration (*Y*) is seen to be strong at Ku band. This suggests the interpretation of mode (1) as the acoustic DR mode and of mode (2) as the optic DR mode. The reduction of the intensity of mode (2) at higher frequencies can be understood through the weaker coupling of the pumping field to this mode. At *K* band, the resonance fields are rather high and the domain magnetization is substantially canted into the film plane. Hence the perturbative torque, $\mathbf{M}\times\mathbf{h}_{rf}$, of the pumping field in configuration (*Y*) decreases and with this the absorbed energy.

• The acoustic mode has to develop into the uniform FMR mode once the domain structure is wiped out by a strong enough in-plane field. From the thickness dependence of mode (1), Fig. 6(a), it is seen that only mode (1) crosses the boundary $H_{sat\|}$ (dashed line) from the stripe domain state to the homogeneously in-plane magnetized state confirming that mode (1) develops from the acoustic DR mode into the uniform FMR mode. This development of mode (1) is clearly pronounced at lower frequencies as shown in Fig. 6(b) for $f=9.2$, 12.6, and 14 GHz. Above 44 nm, in regions I and IIb of Fig. 3, the magnetization processes are dominated by the out plane magnetization component. In this thickness range the resonance field is almost constant and corresponds to the acoustic DR mode excitation. Below 44 nm, regions IIb and III, the in-plane component dominates [compare Fig. 3(c)] and the resonance field rises towards its in-plane uniform mode value.

C. DR modes and high-*Q* 1D model

The frequency-field dispersion of the domain resonance modes can be obtained almost analytically for high-*Q* materials.[18] In this case the domain magnetization of the up and down domains is represented by a 1D macrospin and the domains are separated by negligibly thin 1D Bloch domain walls. For details see Ref. 18.

The frequency-field dispersion as derived from this high-*Q* 1D calculation[18] using the parameters of Co(0001) is shown in Fig. 8(a) for the acoustic and optic DR modes (lines) together with the experimental data ($t=84$ nm) (points). At high frequencies, the calculated acoustic-mode dispersion is continued by the uniform in-plane magnetized dispersion and is in agreement with the experimental data.

The almost quantitative agreement seen at *K*-band frequencies (24 GHz) of the acoustic and optic DR modes of Co(0001) with the high-*Q* model is found for all Co(0001) films in the thickness range I. At *K* band the resonance field has values between 4 and 5 kOe, a field at which the magnetization inside the domains and the flux closure structure has rotated already considerably into the applied field direction and at which the internal demagnetization field H_{dz} does not vary much across the film thickness; see Fig. 4(d). This in-plane canting thus reduces the effect of the flux closure

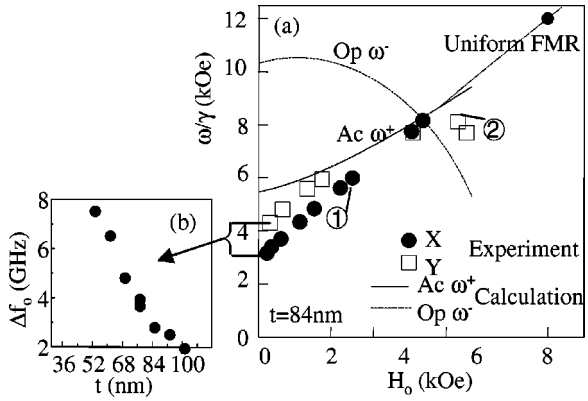

FIG. 8. (a) Comparison of the experimental frequency-field dispersion for $t=84$ nm of the acoustic and optic domain resonance modes (full dots and open squares) with the dispersion calculated from the high-*Q* 1D model (Ref. 18) for ideal stripe domains (lines). (b) Experimental zero-field frequency splitting Δf_0 as a function of film thickness.

caps [see also contour map Fig. 4(c)] and the magnetization distribution approaches that of an ideal stripe domain structure at the respective field value. In this case, the calculation of the high-*Q* model will provide a reasonable estimate for the DR modes, as seen in Fig. 8(a).

In contrast, at low-frequency and field values the flux closure caps are pronounced and strong deviations from the high-*Q* model are expected. Due to the different internal fields inside the domains and the flux closure caps, the latter do not participate in the domain resonance oscillations. Consequently, the domain surface charges remain essentially unaltered in the acoustic-mode precession [compare Fig. 7(a)]. Similarly, the broad flux closure caps reduce the domain-wall surface charging effect for the optic type precession [compare Fig. 7(b)]. In total, the effect of the flux closure caps should be a ''screening''of the dynamic dipolar coupling between the adjacent domains such that they appear dynamically as decoupled. This may explain the experimentally observed near degeneracy of the acoustic and optic DR modes at low fields and frequencies seen in Fig. 8(a). However, this explanation does not hold consistently for all *t*. In Fig. 8(b) the zero-field frequency splitting Δf_0 between the acoustic and optic DR modes shows a relatively strong increase upon reducing *t*. These inconsistencies indicate that other dynamic restoring torques must be present which modify the precession frequency. These may arise for example from the inhomogeneous demagnetization fields H_{dz} as shown in Fig. 4(d), which vary parabolically across the film thickness at low field values and can give rise to an inhomogenous precession amplitude and thus to additional dynamic exchange and dipolar torques.

VII. DOMAIN-WALL RESONANCE MODES AND FLUX CLOSURE EXCITATIONS

A. Bloch wall resonance and flexure modes

Domain-wall resonance. The second type of excitations in a stripe domain structure is the oscillation of the domain

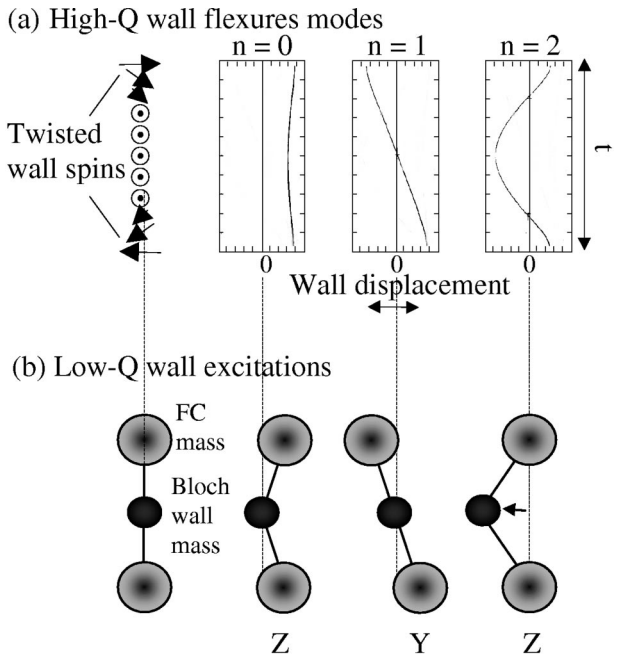

FIG. 9. (a) The three lowest order flexure type oscillations of high-Q twisted wall structures (from Ref. 27). In the $n=0$ mode, the amplitude of the wall oscillation is larger at the surface than in the film center, whereas it is reversed in the case of $n=2$. For the $n=1$ mode, the wall parts at the top and bottom surface oscillate in opposite directions. (b) The corresponding wall resonance modes of low-Q flux closure stripe domains.

wall[14,16,18,20] as a whole around its equilibrium position at a frequency $\omega=\sqrt{k/m}$. Here k is a restoring force constant and m an effective wall mass. In the stripe domain structure, a displacement of the domain wall from its equilibrium position disturbs the balance of the demagnetization fields, resulting in a pressure on the wall which will drive it back into its equilibrium position[14,20] (restoring pressure). Furthermore, the energy of a wall moving at velocity v is increased with respect to the resting wall.[14,15] This additional energy can be expressed in form of a kinetic energy, denoting that a moving wall contains an inertia or inertial mass m.[14,15,20] Hence the wall can perform harmonic oscillations when excited in a perpendicular pumping configuration (Z) as shown in Fig. 1.

Flexure modes. Even for high-Q materials slight deviations from the pure Bloch domain-wall structure exist at the film surface where the wall spins are twisted perpendicular to the wall plane,[14,16] see Fig. 9(a). However, these deviations can be considered as a small perturbation of the domain-wall structure along the thickness without a substantial broadening of the wall. Slonczewski[16] has shown that in this case the domain wall can undergo flexural-type oscillations where the oscillation amplitude varies across the film thickness. The three lowest order modes are indicated in Fig. 9(a). These modes have been confirmed experimentally for high-Q garnet films.[26–28]

Since the domain-wall mass m depends sensitively on the internal wall energy[14,15,20,29] and thus on the total domain-wall profile, the pronounced flux closure caps in the low-Q

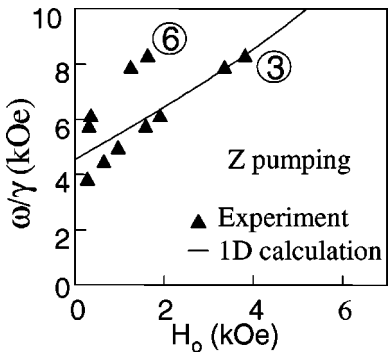

FIG. 10. Comparison of the experimental frequency-field dispersion for $t=84$ nm for modes (3) and (6) excited in configuration Z (full triangles) with the dispersion of the Bloch domain-wall resonance mode calculated from the high-Q 1D model (Ref. 18) for ideal stripe domains (line).

Co(0001) films must be described by a wall mass differing from the one of the Bloch part in the film center. This is illustrated schematically in Fig. 9(b). With this, two almost independent modes should be excited in pumping configuration (Z), a Bloch domain-wall resonance (BDWR) as well as a flux closure resonance (FCR). They can be regarded as an extreme limit of the $n=0$ and $n=2$ flexure modes for high-Q materials,[16] see Fig. 9(b), with $n=0$ corresponding to an oscillation dominated by the flux closure caps and $n=2$ corresponding to an oscillation dominated by the Bloch part. Similarly, in configuration (Y), the analog of the $n=1$ flexure mode is predicted, which involves an asymmetrical displacement (shearing) of the top and bottom flux closure caps. This mode is therefore called the ''flux closure shearing mode.'' These three modes are indicated in the pumping scheme of Fig. 1 in the respective configurations (Y) and (Z).

Comparison to experiment. In the experiment two modes (3) and (6) are excited in pumping configuration (Z) and two modes (2) and (5) in configuration (Y), where mode (2) is identified as the optic DR mode. From these excitations, mode (3) is associated with the domain-wall resonance mode by the following comparison.

In region I, the resonance fields of mode (3) have values between 3 and 4 kOe; see Fig. 6(a). Similarly to the conclusions drawn for the DR modes, in this field range the magnetization is substantially canted towards the bias field direction (in plane and parallel to the stripes) inside the domains as well as inside the flux closure caps. With this, the Néel-like structure of the flux closure caps transforms into a Bloch-like structure and the magnetization profile of the domain wall is smoothed across the film thickness and approaches the 1D Bloch wall configuration at the respective field value. In particular, as seen from the 2D micromagnetic calculation Fig. 4(c), the effective Bloch wall height increases. Hence, for the Co(0001) films at high fields (frequencies) and for $t>60$ nm, a reasonable estimate of the resonance frequencies should be provided by the high-Q 1D calculation of the BDWR.[18] These can be derived using an approach similar to the one indicated in Sec. VI C for the domain resonance modes, (see Ref. 18 for details). In Fig. 10 this high-Q 1D calculation is compared to the frequencies of

modes (3) and (6) excited in configuration (Z). The calculated frequencies are close to mode (3) at high frequencies and fields. This agreement is found for all samples in region I for $t>60$ nm, as shown in Fig. 6(a) by the full line through mode (3), and suggests that at high frequencies mode (3) can be described by the formalism of the Bloch domain-wall resonance.

Below 60 nm, the onset of the in-plane canting of the domain magnetization at zero field, see Fig. 4(a), accompanied by a broadening of the Bloch wall part will change the restoring forces as well as the domain-wall mass. This explains qualitatively the drastic change in the slope of mode (3) below 60 nm in Fig. 6(a). Similarly, the deviations from the calculations in Fig. 10 at low field (and frequencies) reflect that at low field the flux closure caps are well pronounced and will be described by a wall mass different from the Bloch part. Upon reducing the field the BDWR will then develop into either a dominant Bloch or a dominant flux closure cap resonance, compare Fig. 9. In light of the short Bloch domain-wall height at zero field shown in Fig. 4(c), it is more likely that the oscillation is dominated by the flux closure domains. This would be consistent with the decrease of the resonance frequency in Fig. 10, indicating an increase in the wall mass.

B. FC core resonance

As shown in Fig. 4(b), the volume fraction of the flux closure core (FC core) at zero field is of the order of 5–6 % for $t>60$ nm. This flux closure core is an almost domainlike region with a dominant m_x component which is sufficiently large to give rise to a measurable FMR absorption peak. The corresponding resonance is referred to as the ''flux closure core resonance'' and can be excited in the pumping configurations (Y) and (Z). In configuration (Z), this is an acoustic-type precession and in configuration (Y) this is an optic-type precession, leading to small differences in dipolar coupling fields. The precessional motion is indicated in Fig. 1 at the bottom of the pumping configuration (Z).

Looking at the frequency and thickness dependence of mode (5) [excited in configuration (Y)] and mode (6) [excited in configuration (Z)] it is observed that the resonance fields of these two modes lie always very close, in particular they show the same thickness dependence, see Fig. 6(a). This indicates a related mode character such as is expected for the domain resonancelike precession of the FC core. Furthermore, the drop of the resonance field to zero below $t=60$ nm of these two modes, Fig. 6(a), is consistent with the drop of the FC core volume obtained from the micromagnetic calculations; see Figs. 4(a) and 4(b). This drop of H_{res} contrasts the behavior of the domain-wall resonance mode (3), which continues to exist well below 60 nm.

The resonance frequency for the FC core mode can be estimated for zero bias H_0 in analogy to the frequency of a homogeneoulsy in-plane magnetized film by $\omega/\gamma=\sqrt{H_{dx}(H_{dx}-H_{eff})}$. Here, H_{eff} is the effective perpendicular uniaxial anisotropy field $H_{eff}=H_u-4\pi M_s$. H_{dx} represents an additional in-plane uniaxial field given by the demagnetization field due to the film surface charges and the flux closure volume charges. It is responsible for the in-plane orientation of the magnetization along the x direction inside the flux closure core. From the experiment, ω/γ extrapolated to zero field lies in the range of 5–6 kOe, from which a demagnetization field H_{dx} of 2–3 kOe is calculated using the above relation. This is of the order of the demagnetization fields obtained from the 2D micromagnetic simulations. The region with $H_{dx}>2$ kOe corresponds roughly to the region of $m_x>0.9$ defined as the FC core. However, it should be noted that this is only a very rough estimate, and that H_{dx} is inhomogeneous taking values of up 6 kOe at the film surface.

C. FC shearing mode

Having associated in configuration (Y) mode (2) with the optic DR mode and mode (5) with the FC core resonance leaves the FC shearing mode [see Fig. 1 (Y)], derived from the analogy of the $n=1$ flexure mode Fig. 9, still to be substantiated experimentally. Since no additional excitation in this configuration (Y) is found up to K band, this indicates that the corresponding resonance frequency at which such a mode sets in lies somewhere in the range between 24 GHz (upper K band) and 34 GHz (Q band). Such high frequencies may be related to the shearing of the flux closure caps which increases the tension of the Bloch walls.

D. FC breathing mode

Similarly to the pumping field (Z) which increases and decreases periodically the up and down domain sizes, a pumping field (X) will periodically increase and decrease the size of the flux closure core. This leads to an oscillation of the two 90° subdomain walls, separating the flux closure core from the domain regions. This mode is indicated by the dotted line in Fig. 1 (X) and is referred to as the ''cap breathing mode.''

From the pumping scheme of Fig. 1 (X) two modes are predicted, but experimentally three modes were evidenced. Having associated mode (1) with the acoustic DR mode, leaves either mode (4) or mode (7) to be associated with the FC breathing mode. The origin of the third mode in this configuration is currently not clear. It is noted though, that recent experiments on FePd thin films[21] reveal a very similar sequence of three resonance absorption peaks in configuration (X), demonstrating the generality of the existence of such modes. Furthermore it is noted that at low fields the very inhomogeneous internal demagnetization field H_{dz} inside the domains, indicated by the contour plot Fig. 4(d), can give rise to an inhomogeneous precession amplitude in the normal acoustic and optic mode. Furthermore, it can give rise to the possibility of the excitation of higher-order modes whose precession frequency is determined by contributions from dynamic exchange or dipolar fields. An example for such a situation was described earlier in Ref. 30.

VIII. SUMMARY

An experimental approach based on ferromagnetic resonance is described for the study of the linear (small amplitude) dynamics of nonhomogeneous magnetization distribu-

tions. Ferromagnetic resonance is a well suited technique to study such excitations, since by means of the conditions $\mathbf{M} \times \mathbf{h}_{rf} \neq 0$ of Sec. IV A and $\mathbf{m}_{tot} \cdot \mathbf{h}_{rf} \neq 0$ of Sec. VI A, a variation of the pumping field orientation permits us to selectively excite different fundamental modes and thus to selectively obtain information on the properties related to regions as small as domain walls. Applying the concept to the flux closure stripe domain structure, a number of excitations are derived which are summarized in the pumping scheme of Fig. 1. Some of these modes bear resemblance to the flexural modes of the high-Q materials, Fig. 9, but also new modes are predicted due to the extended nature of the walls.

From the experiment, performed for different pumping field orientations and as a function of pumping field frequency and film thickness, a rich excitation spectrum is evidenced for the Co(0001) stripe domain structure. The observed modes can be classified according to the pumping scheme of Fig. 1 in combination with the information obtained from the static properties obtained from MFM imaging, SQUID magnetometry, and static 2D micromagnetic simulations.

While a qualitative description of these modes is given, a quantitative description of the frequency-field dispersion is missing, requiring new approaches which go beyond the existing analytic 1D high-Q model[18] and the static 2D micromagnetic simulations used here. First results have been reported recently[31] for the zero-field excitations using dynamical 2D micromagnetic simulations, which need to be extended to include the field dependence. A quantitative evaluation of the observed spectra will then provide a means to evidence and analyze complex magnetization distributions not accessible by current domain imaging techniques.

ACKNOWLEDGMENTS

This work was partially supported by the NSF program INT-9972538 and by the R. Yeh fund (U.E. and P.E.W.), as well as by the NSF-CNRS-9603252 program and the EC program Training and Mobility of Researchers ''Dynaspin'' FMRX-CT97-0124 (U.E. and K.O.).

APPENDIX: 2D MICROMAGNETIC CALCULATIONS

For the calculation of the magnetization distribution of the Co stripe domain structure, a discretization scheme introduced by LaBonte[32] was used. The discretization consists of infinitely long square prism with a discretization lattice constant of 2 nm, which is smaller than the exchange length for Co (4.9 nm). The magnetization was taken constant inside each prism cell. The magnetization distribution was obtained upon numerical integration of the Landau-Lifschitz-Gilbert equation with respect to time, using for the damping constant $\alpha = 1$ since only quasistatic solutions are of interest. The integration was performed using the explicit Euler method (forward time). At the free surfaces, the Neumann boundary condition were imposed. The demagnetization field was calculated using fast Fourier transforms. The corresponding coefficients of the demagnetization field were modified according to Ref. 33 in order to include the periodicity of the stripe domain structure. The calculation was stopped, when the maximum torque was smaller than a prescribed tolerance. Since for each configuration, the domain width L (or period $2L$) is an input parameter, L was determined upon calculating the total energy as a function of L. The optimum domain width is then given by the minimum of total energy.

[1] See, for example, A. Hubert and R. Schäfer, in *Magnetic Domains* (Springer, New York, 1998), Chap. 5.5.4 and references therein.

[2] B. Hillebrands, in *Light Scattering in Solids VII*, Topics in Applied Physics Vol. 75, edited by M. Cardona and G. Güntherodt (Springer-Verlag, Berlin, 2000).

[3] J. F. Cochran, in *Ultrathin Magnetic Structures*, edited by. B. Heinrich and J. A. C. Bland (Springer-Verlag, Berlin, 1994), Chap. 3.2 and references therein; *ibid.*, Chap. 3.3.

[4] B. Heinrich, in *Ultrathin Magnetic Structures* (Ref. 3), Chap. 3.1, and references therein.

[5] M. Farle, Rep. Prog. Phys. **61**, 755 (1998).

[6] M. Hehn, S. Padovani, K. Ounadjela, and J. P. Bucher, Phys. Rev. B **54**, 3428 (1996).

[7] A. Hubert and R. Schäfer, in *Magnetic Domains* (Ref. 1), Chap. 3.7.4; A. Hubert and W. Rave, J. Magn. Magn. Mater. **196**, 325 (1999).

[8] M. Labrune and J. Miltat, IEEE Trans. Magn. **26**, 1521 (1990).

[9] U. Ebels, P. E. Wigen, and K. Ounadjela, Europhys. Lett. **46**, 94 (1999).

[10] C. Kittel, Phys. Rev. **70**, 965 (1946).

[11] C. Koy and U. Enz, Philips Res. Rep. **15**, 7 (1960); Z. Malek and V. Kambersky, Czech. J. Phys., Sect. A **8**, 416 (1958).

[12] For comparison of the structural and static magnetic properties, see Ref. 6, which describes the same Co(0001) system, the only difference being the substrate material, which is sapphire in Ref. 6, vs. mica in this work. A comparison of films grown on both substrate materials revealed no influence of the substrate material on the magnetostatic properties or on the excitation spectrum.

[13] See, for example, Eqs. (6) and (7) in C. Chappert, K. Le Dang, P. Beauvillain, H. Hurdequint, and D. Renard, Phys. Rev. B **34**, 3192 (1986).

[14] A. P. Malozemoff and J. C. Slonczewski, *Magnetic Domain Walls in Bubble Materials* (Academic Press, New York, 1979).

[15] J. C. Slonczewski, Int. J. Magn. **2**, 85 (1972); J. Appl. Phys. **44**, 1759 (1973).

[16] J. C. Slonczewski, J. Magn. Magn. Mater. **23**, 305 (1981).

[17] S. Smit and S. Beljiers, Philips Res. Rep. **10**, 113 (1955); J. O. Artman and S. H. Charap, J. Appl. Phys. **49**, 1587 (1978).

[18] M. Ramesh and P. E. Wigen, J. Magn. Magn. Mater. **74**, 123 (1988).

[19] B. Luhrmann, H. Dötsch, and S. Sure, Appl. Phys. A: Solids Surf. **A57**, 533 (1993).

[20] J. Morkowski, H. Dötsch, P. E. Wigen, and R. J. Yeh, J. Magn. Magn. Mater. **25**, 39 (1981).

[21] N. Vukadinovic, H. Le Gall, J. Ben Youssef, V. Gehanno, A. Marty, Y. Samson, and B. Gilles, Eur. Phys. J. B **13**, 445 (2000).
[22] Y. Shimida, M. Shimoda, and O. Kitakami, Jpn. J. Appl. Phys., Part 1 **34**, 4786 (1995); O. Acher, C. Boscher, B. Brule, G. Perrin, N. Vukadinovic, G. Suran, and H. Joisten, J. Appl. Phys. **81**, 1 (1997).
[23] Z. Frait and D. Fraitova, in *Frontiers in Magnetism of Reduced Dimension Systems*, Vol. 49 of *NATO Advanced Study Institute, Series* 3, edited by V. G. Bar'yakhtar, P. E. Wigen, and N. A. Lesnik (Kluwer, Dordrecht, 1998).
[24] It should be pointed out that the pumping field can penetrate from both sides and that at the resonance of the domain center spins the surface flux closure spins are off resonance and therefore do not contribute to the skin depth.
[25] A. Layadi and J. O. Artman, J. Magn. Magn. Mater. **92**, 143 (1990); Z. Zhang, L. Zhou, P. E. Wigen, and K. Ounadjela, Phys. Rev. B **50**, 6094 (1994).
[26] B. E. Argyle, J. C. Slonczewski, W. Jantz, J. H. Spreen, and M. H. Kryder, IEEE Trans. Magn. **MAG-18**, 6 (1982); B. E. Argyle, W. Jantz, and J. C. Slonczewski, J. Appl. Phys. **54**, 3370 (1983).
[27] S. Batra and P. E. Wigen, J. Appl. Phys. **61**, 4207 (1987).
[28] N. Vukadinovic, A. Serraj, H. Le Gall, and J. Ben Youssef, Phys. Rev. B **58**, 385 (1998).
[29] S. W. Yuan and H. N. Bertram, Phys. Rev. B **44**, 12 395 (1991).
[30] A. M. Portis, Appl. Phys. Lett. **2**, 69 (1963).
[31] N. Vukadinovic, O. Vacus, M. Labrune, O. Acher, and D. Pain, Phys. Rev. Lett. **85**, 2817 (2000).
[32] A. E. LaBonte, J. Appl. Phys. **40**, 2450 (1969).
[33] N. Hayatashi, K. Saito, and Y. Nakatani, Jpn. J. Appl. Phys., Part 1 **35**, 6065 (1996).